JACS
JOURNAL OF THE AMERICAN CHEMICAL SOCIETY
Communication
pubs.acs.org/JACS

Magic-Angle-Spinning NMR of the Drug Resistant S31N M2 Proton Transporter from Influenza A

Loren B. Andreas,[†] Matthew T. Eddy,[†] James J. Chou,[‡] and Robert G. Griffin*[,†]

[†]Francis Bitter Magnet Laboratory and Department of Chemistry, Massachusetts Institute of Technology, Cambridge, Massachusetts 02139, United States

[‡]Department of Biological Chemistry and Molecular Pharmacology, Harvard Medical School, Boston, Massachusetts 02115, United States

Supporting Information

ABSTRACT: We report chemical shift assignments of the drug-resistant S31N mutant of $M2_{18-60}$ determined using 3D magic-angle-spinning (MAS) NMR spectra acquired with a $^{15}N-^{13}C$ ZF-TEDOR transfer followed by $^{13}C-^{13}C$ mixing by RFDR. The MAS spectra reveal two sets of resonances, indicating that the tetramer assembles as a dimer of dimers, similar to the wild-type channel. Helicies from the two sets of chemical shifts are shown to be in close proximity at residue H37, and the assignments reveal a difference in the helix torsion angles, as predicted by TALOS+, for the key resistance residue N31. In contrast to wild-type $M2_{18-60}$, chemical shift changes are minimal upon addition of the inhibitor rimantadine, suggesting that the drug does not bind to S31N M2.

The M2 proton transporter from influenza A conducts at low pH and is the target of the aminoadamantyl inhibitors rimantadine (Rmt) and amantadine (Amt), whose activity is believed to arise from binding to the pore of the channel.[1−6] The inhibitors reduce the rate of proton conduction, thereby interfering with the unpacking of the viral particle in the endosomal pathway for infection. However, a single mutation of serine 31 to asparagine (S31N) renders these inhibitors ineffective for many current influenza A infections,[7] and therefore understanding the structure of the S31N mutant and the structural basis for resistance could guide the design of more potent inhibitors that would target current flu variants. In addition, since the S31N mutation is far more prevalent than the commonly studied wild type (WT) Udorn strain of M2, the structure of S31N M2 is more relevant for the design of novel inhibitors that might exploit a new mechanism.

A segment of the protein comprising approximately residues 18−60 of the full 97 amino acid sequence is known to retain the critical function of proton conduction and inhibition by Amt and Rmt.[8,9] Several structures and structural models of WT M2 have been reported using solution NMR spectroscopy,[10] oriented-sample NMR spectroscopy,[5] crystallography,[4] and solid-state NMR spectroscopy combining oriented-sample constraints[11] and magic-angle spinning (MAS).[12] However, there have been few investigations of the S31N mutant. A solution NMR structure of S31N M2 was reported,[9] but it was solved using a detergent and buffer system that did not support Rmt binding in the pore of WT M2. Thus, it appears that M2 structure and inhibition are sensitive to the membrane-mimetic environment. Therefore, an investigation of the S31N variant in fully hydrated lipid bilayers could reveal new functionally relevant structural features.

Additionally, the S31N mutant can be used as a negative control for experiments that investigate the effects of drug binding. It was shown previously that large and widespread chemical shift changes occur upon binding of Rmt to WT $M2_{18-60}$,[13] and similar changes occur in a shorter construct comprising residues 22−46.[14] Since S31N $M2_{18-60}$ is drug-resistant, chemical shift changes due to nonspecific effects should remain upon addition of the drug, and the functionally important chemical shift changes should be absent. Therefore, the S31N mutant can assist in differentiating between binding and nonspecific hydrophobic effects that may be present as a result of the large excess of inhibitor used in the MAS NMR experiments.

Here we report the initial MAS NMR spectra of S31N $M2_{18-60}$ reconstituted into lipid bilayers, from which we can derive interesting details of the channel structure. The spectra of S31N $M2_{18-60}$ at 900 MHz (Figure 1) exhibited high resolution of ∼0.7 and 0.5 ppm for ^{15}N and ^{13}C backbone linewidths, respectively. This allowed all of the strong resonances in this ZF-TEDOR[15,16] spectrum to be assigned on the basis of the primary sequence and sequential correlations in a 3D $^{15}N-^{13}C-^{13}C$ chemical shift correlation experiment using ZF-TEDOR and RFDR[17,18] [see Figures 3 and 4; assignments are shown in Table S2 in the Supporting Information (SI)]. Full assignments were made for 14 of the 43 residues, and an additional seven ^{15}N assignments were made because of transamination of isoleucine and leucine residues, through which these residues were ^{15}N-labeled despite the addition of natural-abundance amino acids prior to protein expression (details below). The ^{13}C signal was suppressed for these residues. A second set of resonances of comparable amplitude (denoted with primes in the figures) were assigned for each residue in the transmembrane region of the peptide between residues 25 and 42, similar to what was observed for WT M2.[13]

This extensive doubling of cross-peaks suggests that the channel assembles as a C_2-symmetric tetramer in a dimer-of-dimers configuration rather than a C_4-symmetric tetramer. The

Received: January 24, 2012
Published: April 5, 2012

dx.doi.org/10.1021/ja3003606 | J. Am. Chem. Soc. 2012, 134, 7215−7218

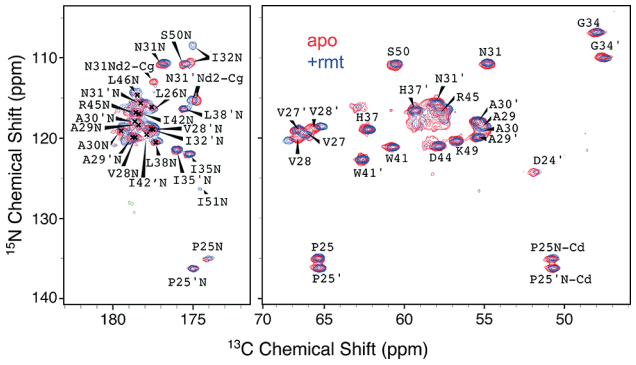

Figure 1. ZF-TEDOR spectra of S31N $M2_{18-60}$ in the presence (blue) and absence (red) of the inhibitor Rmt. The spectra were recorded at a ^{1}H frequency of 900 MHz and demonstrate ^{15}N and ^{13}C backbone linewidths of ~0.7 and ~0.5 ppm, respectively. Labels correspond to N−Cα cross-peaks (right) and nitrogen i of N_i−C_{i-1} cross-peaks (left), unless otherwise indicated. The sample temperature was ~30 °C, the spinning frequency was 20 kHz, and the TEDOR mixing time was 1.2 ms.

C_2 symmetry was previously proposed as the best explanation for the WT spectra, which also demonstrated similar intensities for the two sets of peaks.[13] Nevertheless, there remained the possibility that the doubled peaks were caused by two different populations of protein that happened to have similar intensities. We excluded the possibility of multiple separate tetramer conformations by showing a cross-peak between the two sets of chemical shifts in a 400 ms proton-driven spin diffusion (PDSD) spectrum recorded at 750 MHz (Figure 2 and Figure S6 in the SI). The cross-peak labeled in the figure is between H37 Cδ2 and H37′ Cε1. Since H37 is a pore-facing residue

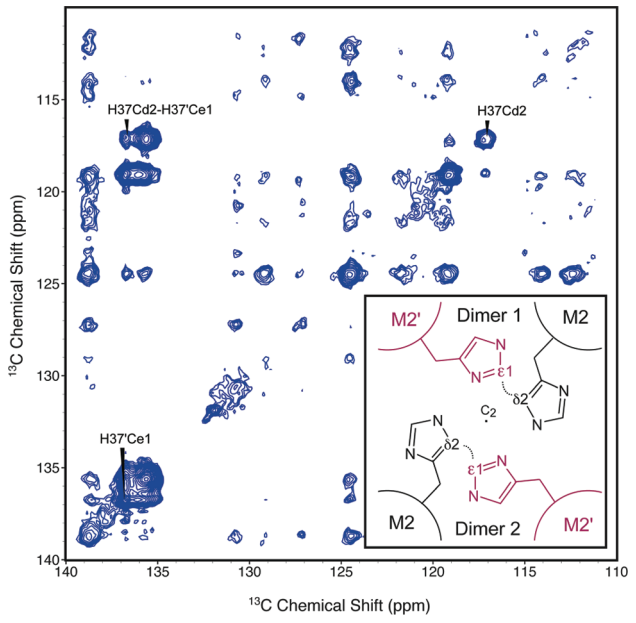

Figure 2. An Aromatic-aromatic ^{13}C correlation spectrum obtained using 400 ms of PDSD mixing shows cross-peaks between the two sets of chemical shifts. The sample temperature was ~10 °C, and the spinning frequency was 14.287 kHz. The inset shows an illustration of a C_2-symmetric channel composed of a dimer of dimers viewed along the C_2 axis with the four α-helices at the corners. The observed intermolecular correlation between carbons δ2 and ε1′ is also depicted in the inset.

known to play a critical role in the ^{1}H selectivity and the pH dependence of ^{1}H conduction,[19,20] we conclude that this cross-peak is within a single tetramer and not a possible tetramer−tetramer contact. In other parts of the molecule, we did not see analogous cross-peaks, indicating that the two sets of shifts do not exchange on this time scale. We therefore conclude that in lipid bilayers, as opposed to detergent, the protein assembles as a C_2-symmetric dimer of dimers on the NMR time scale.

Unlike WT M2, only relatively minor changes in chemical shift (<2 ppm ^{15}N, <1 ppm ^{13}C) were observed upon the addition of a 4-fold molar excess of the inhibitor Rmt. Notably, the ~7 ppm change in the ^{15}N shift of residue 31 and the ~3.5 ppm change in the shift for H37 Cα are absent in S31N M2.[21] The largest chemical shift changes occur for lipid-facing residues such as V28 Cα and I32 ^{15}N that also lie near the lipid headgroups where the amphiphilic Rmt is expected to partition. Since the inhibitor partitions strongly into membranes,[22] it constitutes ~7% of the total membrane components by mass (~35 mol %). Therefore, the shift changes can be attributed to nonspecific differences in the membrane composition upon addition of the drug.

The program TALOS+[23] was used to predict the backbone torsion angles ϕ and ψ for both sets of chemical shifts, and the results are listed in Table S1. Since TALOS+ makes predictions based on sequential amino acid triplets, the current labeling restricted the analysis to the longest stretch of continuously labeled and assigned residues, namely, residues 27−31 (VVAAN). As expected, the results show an α-helical conformation. More interestingly, the two sets of chemical shifts are separated enough to show a difference in the predicted torsion angles. The predicted values of ϕ and ψ differ by 13 and 14°, respectively, for the key resistance residue N31, suggesting that the symmetrically inequivalent helices may have different secondary structures.

The widespread cross-peak doubling and C_2-symmetric structure have thus far been uniquely resolved for the 18−60 construct in lipid bilayers. In solution, only a single set of resonances was observed, indicating that if two conformations exist, they undergo fast exchange on the NMR time scale. This resulted in C_4-symmetric structural constraints.[9] Crystal structures of WT $M2_{22-46}$ showed some conformational heterogeneity, but a C_2 axis was apparently not evident, as channel models based on the crystal structure were constructed with C_4 symmetry.[4] Peak doubling was not resolved by MAS NMR spectroscopy of the shorter 22−46 construct of WT M2,[12] although doubling may be present beneath the significantly broader line widths that were reported for this construct. The dimer-of-dimers topology is in qualitative agreement with a previous MAS NMR study that proposed an imidazole−imidazolium dimer in $M2_{22-46}$,[19] implying C_2 symmetry at H37. However, at pH 7.8, we observed neutral His (based on side-chain nitrogen shifts near 250 ppm; see Figure S1) for both sets of chemical shifts, in contrast to the imidazole−imidazolium dimers, which were reported to form when the tetramer is doubly protonated with a pK_a of 8.2. Nevertheless, it is possible that the previously reported dimerization and the widespread doubling of peaks are manifestations of the same underlying structural feature and that the pK_a is sensitive to the sample differences.

Existing evidence points to several possible modes by which the S31N mutation confers drug resistance. The larger side chain of asparagine might prevent the drug from binding by reducing the space in the pore, and this mode of resistance was

dx.doi.org/10.1021/ja3003606 | J. Am. Chem. Soc. 2012, 134, 7215−7218

supported by surface plasmon resonance measurements in which binding was not observed for the S31N mutant.[24,25] On the other hand, structures solved by solution NMR spectroscopy show residue 31 in the helix−helix interface,[3,9,10] suggesting that the mutation might severely weaken the channel−drug interactions by altering the helix packing. The widespread doubling of resonances and the 13 and 14° differences in the predicted values of ϕ and ψ for N31 suggest that a detailed understanding of the drug-resistant structure may include twofold symmetry for the channel.

Chemical shift assignments were achieved via 3D ^{15}N−^{13}C−^{13}C spectra[26,27] that were obtained using one-bond ^{15}N−^{13}C ZF-TEDOR mixing followed by ^{13}C−^{13}C RFDR mixing, similar to previously described 2D experiments[28] and the commonly used N−C double cross-polarization (DCP)-based experiments.[29−32] The sequence, which is depicted in Figure 3, allows both the NCOCX and NCACX connectivity

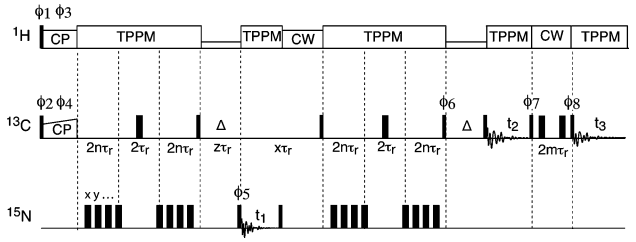

Figure 3. 3D ZF-TEDOR−RFDR pulse sequence used for assignments. Narrow and broad bars represent pulses of 90 and 180° nutation, respectively. Vertical dashed lines indicate rotor synchronization. The parameters n and m determine the total TEDOR and RFDR mixing times, respectively, by extension of the corresponding pulse trains. The phase cycle was ϕ_1 = (16 × 1)(16 × 3), ϕ_2 = (16 × 4)(16 × 2), ϕ_3 = 2, ϕ_4 = 1, ϕ_5 = 13, ϕ_6 = 2244, ϕ_7 = 1133, ϕ_8 = 1111222233334444, and ϕ_{rec} = 4242 1313 2424 3131 2424 3131 4242 1313. The REDOR mixing in ZF-TEDOR and the RFDR mixing used *xy*-4 and *xy*-16 phase alternation, respectively. All other pulses had a phase of 1. The phases of the pulses after t_1 evolution and before t_2 evolution were incremented for phase-sensitive detection. Because of time constraints, only the first four values of the phase cycle were used.

experiments to be acquired efficiently in a single spectrum (Figure 4). Efficient NCACX and NCδCX transfers were demonstrated for Pro, a residue that is often difficult to observe in DCP spectra because of weak H−N cross-polarization to the Pro nitrogen. The ZF-TEDOR transfer avoids this problem because the experiment begins with a H−C cross-polarization step. In principle, this experiment should also provide assignment information originating from side-chain ^{15}N atoms in residues such as histidine, tryptophan, lysine, and arginine. However, we found that these transfer efficiencies were reduced, and their detection would have required significantly longer experiment times. To avoid excessive spectral widths in the indirect ^{13}C dimension, we folded the carbonyl resonances onto the spinning sideband just above the aliphatic resonances by applying a dwell time matching the rotor period. A spinning frequency corresponding to ∼90 ppm was useful for this reduction in the sweep width and also avoided strong rotational resonance conditions.[33−35]

$M2_{18-60}$ was prepared by overexpression in *Escherichia coli* as described previously[10,13] with C19S and C50S mutations to prevent unwanted disulfide bond formation. The resulting sequence with the S31N mutation was RSNDSSDPLV VAANIIGILH LILWILDRLF FKSIYRFFEH GLK. To simplify

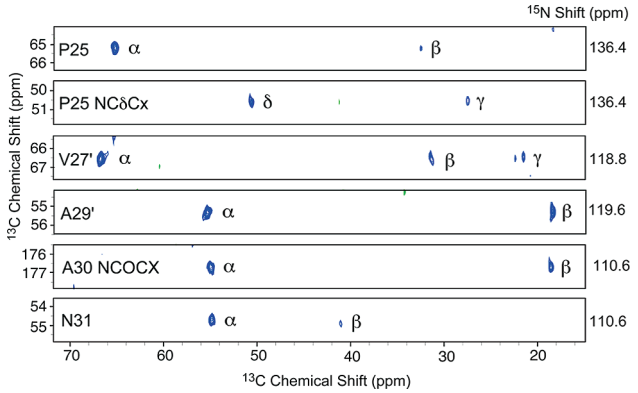

Figure 4. Slices of the NCACX and NCOCX regions of a 3D ZF-TEDOR-RFDR spectrum used for sequential assignments. For P25, the NCδ transfer was also efficient (second panel). TEDOR mixing for 1.2 ms and RFDR mixing for 4.8 ms with 83 kHz pulses were used. The direct acquisition used a 6 μs dwell time and 3072 points (∼18.4 ms), the indirect ^{13}C dimension a 50 μs dwell time and 180 complex points (9 ms), and the ^{15}N dimension 150 μs dwell time and 74 complex points (11.1 ms). The carrier frequency was set to 100 ppm for ^{15}N and 89 ppm for ^{13}C. The spectrum was acquired in ∼5 days and provided useful NCACX and NCOCX connectivity information. The sample temperature was ∼30 °C, and the spinning frequency was 20 kHz.

the spectra, I, L, F, and Y residues were unlabeled by addition of the natural-abundance amino acids to the culture ∼1 h prior to induction in the concentrations of 150, 150, 50, and 100 mg/L, respectively. Bilayer protein samples were prepared by adding 1,2-di-*O*-phytanoyl-*sn*-glycero-3-phosphocholine (DPhPC) lipid (Avanti) and lyophilized $M2_{18-60}$ at a lipid/protein ratio of 1:1 by weight (∼6:1 molar ratio), both dissolved in denaturing buffer [6 M guanidine, 40 mM phosphate, 30 mM glutamate, 3 mM sodium azide (Sigma-Aldrich), pH 7.8, ≥33 mg/mL OG detergent (Anatrace)]. The resulting solution was dialyzed in a 3.5 kD cutoff dialysis cassette (Thermo) against 1 L of sample buffer (40 mM phosphate, 30 mM glutamate, 3 mM sodium azide, pH 7.8) for 7 days with two dialysis buffer changes per day. A white precipitate was observed after ∼24 h. Solid membrane material was pelleted by centrifugation at ∼100000*g*. Samples with Rmt had a 4-fold molar excess added directly to the membrane pellet.

The NMR spectrum in Figure 2 was recorded on a 750 MHz spectrometer courtesy of David Ruben, and all other spectra were recorded using a Bruker 900 MHz spectrometer (Bruker Biospin). Each instrument employed a Bruker 3.2 mm HCN e-free probe. ^{13}C referencing was performed using the chemical shifts of adamantine relative to 4,4-dimethyl-4-silapentane-1-sulfonic acid (DSS),[36] and the relative frequency ratios between DSS (^{13}C) and liquid ammonia (^{15}N)[37,38] were used for ^{15}N referencing. The sample temperature was estimated using the chemical shift of ^{79}Br in KBr to determine the heating due to sample spinning.[39] (See Figure S2 for a comparison of spectra recorded at 10 and 30 °C, the temperatures used for PDSD and assignment, respectively.) Spectra were processed with NMRPipe[40] and displayed and assigned using Sparky.[41]

We have shown that a single 3D ZF-TEDOR−RFDR spectrum acquired in 5 days is sufficient for sequential assignment of reverse-ILFY-labeled S31N $M2_{18-60}$. Minor differences in chemical shifts were observed upon addition of inhibitor, and the absence of the dramatic shift changes seen for

dx.doi.org/10.1021/ja3003606 | J. Am. Chem. Soc. 2012, 134, 7215−7218

WT M2 confirm their functional significance. The assignments revealed two distinct sets of resonances that were shown by PDSD mixing to be in close contact, from which we conclude that the tetramer assembles as a C_2-symmetric dimer of dimers with two symmetrically inequivalent helices. The predicted TALOS+ geometry of the two helices was also found to be distinct, particularly for the resistance residue N31. These structural features observed in lipid bilayers provide clues to the mechanism of resistance, and further structural investigation of drug-resistant M2 could provide a starting point for the design of more potent or novel inhibitors.

■ ASSOCIATED CONTENT

Supporting Information

Table of torsion angles predicted using TALOS+, chemical shift assignment table, spectrum showing the protonation state of H37, $^{13}C-^{13}C$ spectra at 10 and 30 °C, peak doubling and drug-induced shift changes as a function of residue number, and a reproduction of Figure 2 with aromatic assignments labeled. This material is available free of charge via the Internet at http://pubs.acs.org.

■ AUTHOR INFORMATION

Corresponding Author

rgg@mit.edu

Notes

The authors declare no competing financial interest.

■ ACKNOWLEDGMENTS

This work was supported by NIH Grants EB-001960, EB-002026, AI-067438, and GM-094608. We thank Rafal Pielak and Marcelo Berardi for thoughtful discussions.

■ REFERENCES

(1) Cady, S. D.; Schmidt-Rohr, K.; Wang, J.; Soto, C. S.; DeGrado, W. F.; Hong, M. *Nature* **2010**, *463*, 689.
(2) Jing, X.; Ma, C.; Ohigashi, Y.; Oliveira, F. A.; Jardetzky, T. S.; Pinto, L. H.; Lamb, R. A. *Proc. Natl. Acad. Sci. U.S.A.* **2008**, *105*, 10967.
(3) Pielak, R. M.; Oxenoid, K.; Chou, J. J. *Structure* **2011**, *19*, 1655.
(4) Stouffer, A. L.; Acharya, R.; Salom, D.; Levine, A. S.; Di Costanzo, L.; Soto, C. S.; Tereshko, V.; Nanda, V.; Stayrook, S.; DeGrado, W. F. *Nature* **2008**, *451*, 596.
(5) Sharma, M.; Yi, M.; Dong, H.; Qin, H.; Peterson, E.; Busath, D. D.; Zhou, H. X.; Cross, T. A. *Science* **2010**, *330*, 509.
(6) Yi, M.; Cross, T. A.; Zhou, H. X. *J. Phys. Chem. B* **2008**, *112*, 7977.
(7) Bright, R. A.; Shay, D. K.; Shu, B.; Cox, N. J.; Klimov, A. I. *JAMA* **2006**, *295*, 891.
(8) Ma, C.; Polishchuk, A. L.; Ohigashi, Y.; Stouffer, A. L.; Schon, A.; Magavern, E.; Jing, X.; Lear, J. D.; Freire, E.; Lamb, R. A.; DeGrado, W. F.; Pinto, L. H. *Proc. Natl. Acad. Sci. U.S.A.* **2009**, *106*, 12283.
(9) Pielak, R. M.; Schnell, J. R.; Chou, J. J. *Proc. Natl. Acad. Sci. U.S.A.* **2009**, *106*, 7379.
(10) Schnell, J.; Chou, J. *Nature* **2008**, *451*, 591.
(11) Hu, J.; Asbury, T.; Achuthan, S.; Li, C.; Bertram, R.; Quine, J. R.; Fu, R.; Cross, T. A. *Biophys. J.* **2007**, *92*, 4335.
(12) Cady, S. D.; Schmidt-Rohr, K.; Wang, J.; Soto, C. S.; Degrado, W. F.; Hong, M. *Nature* **2009**, *463*, 689.
(13) Andreas, L. B.; Eddy, M. T.; Pielak, R. M.; Chou, J.; Griffin, R. G. *J. Am. Chem. Soc.* **2010**, *132*, 10958.
(14) Cady, S. D.; Mishanina, T. V.; Hong, M. *J. Mol. Biol.* **2009**, *385*, 1127.
(15) Jaroniec, C. P.; Filip, C.; Griffin, R. G. *J. Am. Chem. Soc.* **2002**, *124*, 10728.
(16) Hing, A. W.; Vega, S.; Schaefer, J. *J. Magn. Reson.* **1992**, *96*, 205.
(17) Bennett, A. E.; Ok, J. H.; Griffin, R. G.; Vega, S. *J. Chem. Phys.* **1992**, *96*, 8624.
(18) Bennett, A. E.; Rienstra, C. M.; Griffiths, J. M.; Zhen, W. G.; Lansbury, P. T.; Griffin, R. G. *J. Chem. Phys.* **1998**, *108*, 9463.
(19) Hu, J.; Fu, R.; Nishimura, K.; Zhang, L.; Zhou, H. X.; Busath, D. D.; Vijayvergiya, V.; Cross, T. A. *Proc. Natl. Acad. Sci. U.S.A.* **2006**, *103*, 6865.
(20) Wang, C.; Lamb, R. A.; Pinto, L. H. *Biophys. J.* **1995**, *69*, 1363.
(21) Cady, S. D.; Luo, W.; Hu, F.; Hong, M. *Biochemistry* **2009**, *48*, 7356.
(22) Wang, J. F.; Schnell, J. R.; Chou, J. J. *Biochem. Biophys. Res. Commun.* **2004**, *324*, 212.
(23) Shen, Y.; Delaglio, F.; Cornilescu, G.; Bax, A. *Journal of Biomolecular Nmr* **2009**, *44*, 213–223.
(24) Astrahan, P.; Kass, I.; Cooper, M. A.; Arkin, I. T. *Proteins: Struct., Funct., Bioinf.* **2004**, *55*, 251.
(25) Rosenberg, M. R.; Casarotto, M. G. *Proc. Natl. Acad. Sci. U.S.A.* **2010**, *107*, 13866.
(26) Sun, B.-Q.; Rienstra, C. M.; Costa, P. R.; Williamson, J. R.; Griffin, R. G. *J. Am. Chem. Soc.* **1997**, *119*, 8540.
(27) Rienstra, C. M.; Hohwy, M.; Hong, M.; Griffin, R. G. *J. Am. Chem. Soc.* **2000**, *122*, 10979.
(28) Riedel, K.; Leppert, J.; Ohlenschlager, O.; Gorlach, M.; Ramachandran, R. *J Biomol NMR* **2005**, *31*, 49.
(29) Ladizhansky, V.; Jaroniec, C. P.; Diehl, A.; Oschkinat, H.; Griffin, R. G. *J. Am. Chem. Soc.* **2003**, *125*, 6827.
(30) Rienstra, C. M.; Hohwy, M.; Mueller, L. J.; Jaroniec, C. P.; Reif, B.; Griffin, R. G. *J. Am. Chem. Soc.* **2002**, *124*, 11908.
(31) Baldus, M.; Petkova, A. T.; Herzfeld, J.; Griffin, R. G. *Molecular Physics* **1998**, *95*, 1197–1207.
(32) Castellani, F.; van Rossum, B. J.; Diehl, A.; Rehbein, K.; Oschkinat, H. *Biochemistry* **2003**, *42*, 11476.
(33) Raleigh, D. P.; Harbison, G. S.; Neiss, T. G.; Roberts, J. E.; Griffin, R. G. *Chem. Phys. Lett.* **1987**, *138*, 285.
(34) Raleigh, D. P.; Levitt, M. H.; Griffin, R. G. *Chem. Phys. Lett.* **1988**, *146*, 71.
(35) Levitt, M. H.; Raleigh, D. P.; Creuzet, F.; Griffin, R. G. *J. Chem. Phys.* **1990**, *92*, 6347.
(36) Morcombe, C. R.; Zilm, K. W. *J. Magn. Reson.* **2003**, *162*, 479.
(37) Markley, J. L.; Bax, A.; Arata, Y.; Hilbers, C. W.; Kaptein, R.; Sykes, B. D.; Wright, P. E.; Wuthrich, K. *J Biomol NMR* **1998**, *12*, 1.
(38) Harris, R. K.; Becker, E. D.; Cabral de Menezes, S. M.; Goodfellow, R.; Granger, P. *Solid State Nucl. Magn. Reson.* **2002**, *22*, 458.
(39) Thurber, K. R.; Tycko, R. *J. Magn. Reson.* **2009**, *196*, 84.
(40) Delaglio, F.; Grzesiek, S.; Vuister, G. W.; Zhu, G.; Pfeifer, J.; Bax, A. *J Biomol NMR* **1995**, *6*, 277.
(41) Goddard, T. D.; Kneller, D. G. *Sparky* 3; University of California: San Francisco, 2008.